ЯДЕРНА ФІЗИКА
NUCLEAR PHYSICS

УДК 539.142 https://doi.org/10.15407/jnpae2024.04.331

B. Rohila[1], N. Kaur[2,*]

[1] *Department of Physics, Maitreyi College, University of Delhi, Delhi, India*
[2] *S. A. Jain College, Ambala City, Haryana, India*

*Corresponding author: nvneet86@gmail.com

HIGH SPIN STRUCTURE IN ^{140}Sm

High spin states of ^{140}Sm have been populated using the ^{116}Cd (^{28}Si, 4n) ^{140}Sm heavy ion fusion evaporation reaction. The previously reported level scheme has been considerably modified and extended. Spin and parity assignments have been made using the DCO and IPDCO methods. Multi-quasiparticle configurations have been assigned to various $\Delta I = 1$ and $\Delta I = 2$ bands based on systematic. A band structure similar to ^{140}Sm has been found in ^{136}Ce. So, the alignments in both the nuclei are compared for various band structures having similar band head spin. This helps in assigning the configuration to various band structures. Level structures have been discussed in the framework of the tilted axis cranking model. Lifetimes of states have been measured using the DSAM method.

Keywords: γ-γ coincidence, Indian National Gamma Array (INGA), spectroscopy, RDCO, DSAM.

1. Introduction

Spectroscopic investigations of nuclei with neutron number below 82 shell closure are important, experimentally as well as theoretically, for the understanding of the various excitation mechanisms responsible for the generation of both low and high spin states in nuclei in this mass region. In the A = 130 - 150 region, a variety of minima corresponding to spherical or near-spherical, low-deformation oblate or prolate, triaxial, and superdeformed shapes have been observed in potential energy surface calculations [1]. The nuclei with A ≈ 140 having a few holes in the N = 82 shell closure are spherical or only slightly deformed in the ground states and can be easily polarized by unpaired nucleons resulting from broken pairs. For the nuclei, there also exists a competition between the differing shape driving effects of the protons and neutrons. The occupied $h_{11/2}$ proton orbitals, being in low-omega orbitals, tend to favour prolate shapes with $\gamma = 0°$ and neutron orbitals tend to favour oblate shapes with $\gamma = -60°$ because they are in high-omega orbitals of $h_{11/2}$. Both the associated prolate and oblate potential-energy minima are predicted to have similar energies [2] which can drive the nuclear shape toward triaxiality. Moreover, due to the availability of particles and holes in the $h_{11/2}$ orbitals, phenomena such as magnetic rotation would be expected as possible mechanisms for the generation of angular momentum. Indeed, several dipole bands, interpreted as magnetic rotational bands [3, 4], have been observed in this mass region. Interesting features such as the coexistence of prolate and oblate collective bands, the transition from collective prolate to non-collective oblate shapes have also been observed.

The high spin states in these nuclei have been populated using the fusion evaporation reactions. The experiments have been performed at the Tata Institute of Fundamental Research (TIFR), Mumbai, using the Indian National Gamma Array (INGA) [5]. Clover detectors of the INGA have been used as polarimeters to decide the nature of the transitions of interest.

2. Experimental details

In the present work, high spin states of ^{140}Sm have been populated using the ^{116}Cd (^{28}Si, 4n) ^{140}Sm heavy ion fusion evaporation reaction at a beam energy of 128.7 MeV provided by pelletron linac at TIFR, Mumbai, India. The target used in the experiment was 1 mg/cm^2 thick ^{116}Cd backed with 6 mg/cm^2 gold foil. The compound nucleus recoil velocity was 1.9 % velocity of light, and the recoil energy was 25 MeV.

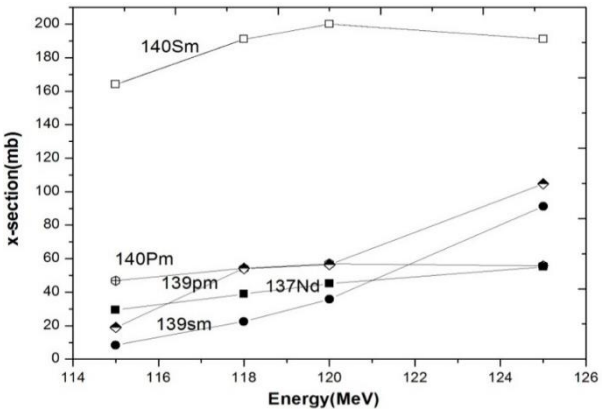

Fig. 1. Various channels populated in ^{116}Cd + ^{28}Si reaction.

INGA [5] consisting of nineteen Compton-suppressed Clover detectors at angles of –23°, –40°, –65°, 90°, 65°, 40°, and 23° was used to detect de-exciting γ-rays. The total number of events recorded was 500 million. The calculated cross-sections using code CASCADE [6] for various channels populated in this reaction are shown in Fig. 1.

3. Data analysis

Two and higher fold γ-γ coincidence list mode data were recorded in a fast digital data acquisition system based on Pixie-16 modules of XIA LLC [7]. The data sorting routine MARCOS (Multi-pARameter time-stamp based COincidence Search program), developed at TIFR, sorts the time-stamped data to generate the E_γ-E_γ matrix and E_γ-E_γ-E_γ cube. The RADWARE [8] software package was used for the analysis of these matrices.

4. Results and discussion

In even-even nuclei with mass A~140, the alignment of proton and neutron quasiparticles in the $h_{11/2}$ orbitals generates low-lying 10^+ states which are in many cases isomeric. These excitations have been observed in the N = 78, ^{140}Sm [9] and ^{142}Gd [10] nuclei. In the rare-earth region, high-j $h_{11/2}$ unique parity orbital is accessible to both neutron and proton excitation. In nuclei of this region, both proton and neutron are in the same high-j shell, i.e. $h_{11/2}$ orbitals which allow us to study the role of p-n interaction and its influence on both collective as well as single particle motion.

For N = 78 nuclei, e.g., ^{142}Gd, ^{138}Nd, ^{136}Ce [10 - 12], the active orbitals for protons and neutrons are $h_{11/2}$, $d_{5/2,}$ and $g_{7/2}$. At low spins, the presence of isomers based on simple particle-hole excitations helps to establish the active quasiparticle configurations and test the suitability of various nuclear potentials. The neutron-deficient rare earth nuclei are an ideal testing ground for theoretical models and the effective nucleon-nucleon interactions that they employ. Previously ^{140}Sm was studied by S. Lunardi et al. [9] using ^{114}Cd(^{30}Si, 4nγ)^{140}Sm reaction at 130 MeV and a cascade of ΔI = 2 transitions based on 10^+ isomer was reported. An interpretation in terms of the coexistence of the two shapes, which are supposed to have different quadrupole deformations, has been suggested. Lifetime measurements in the collective sequences found above the two isomers can give a more definite answer to the question of the coexistence of different nuclear deformations. Earlier, M.A. Cardona [13] reported a lifetime of a few states above 10^+ states by means of the recoil-distance Doppler-shift technique, using a precision plunger apparatus.

Excited levels in ^{140}Sm were populated using the ^{106}Pd(^{37}Cl, p2n)^{140}Sm reaction at a bombarding energy of 143 MeV [13]. In the present work, the level scheme has been extended with the addition of several new transitions. The band structure and deformation are discussed in the framework of the tilted axis cranking model (TAC). The lifetimes of a few states have been measured using the DSAM method. The level scheme of ^{140}Sm shown in Fig. 2 is based on γ-ray coincidence and intensity relationships. Much of the level scheme of previous work has been verified along with certain modifications and additions. The level scheme of ^{140}Sm has been modified with the addition of several new γ-rays. Fig. 2 displays various positive and negative parity bands labelled from 1 to 11. Newly found transitions are marked by an asterisk. The properties of the transitions extracted in this work are listed in Table 1.

The placement of new transitions in bands 2 and 3 is confirmed by setting double gates on 531, 952 keV γ-rays and 782, 808 keV γ-rays in cube (Fig. 3). The γ-ray coincidence spectrum shown in Fig. 4 is obtained by setting double gates on the $7^- \rightarrow 5^-$ (312 keV) and $5^- \rightarrow 4^+$ (769 keV) transitions in ^{140}Sm and it shows all the γ transitions connecting to 5^- state.

5. Spin and parity assignments

Multipolarities of the γ-ray transitions were determined using the RDCO method [14]. An asymmetric matrix was created using MARCOS with the events detected by Clovers at 90° on one axis and Clovers at 157° on the other axis. The following relation was used for the calculation of RDCO ratios:

$$RDCO = \frac{I\left(\gamma_1 : 157° \, gated by \, \gamma_2 : 90°\right)}{I\left(\gamma_1 : 90° \, gated by \, \gamma_2 : 157°\right)}. \qquad (1)$$

In order to obtain information about the levels of parities, linear polarization measurements were performed using the IPDCO method [15]. In Fig. 5, spectra containing parallel and perpendicular events are compared by putting a gate on 442 keV γ-ray in band 6. Black lines in the spectrum correspond to perpendicular events and red line corresponds to parallel events. From the intensity comparison, we can conclude that 305, 317, 373, and 378 keV γ-rays are magnetic in nature, and band 5 has been assigned negative parity. The 241 keV γ-ray seems to be electric in nature. By gating on 619 keV γ-ray, we observed 306, 366, and 454 keV transitions of band 8 (see Fig. 2) and found them magnetic in nature.

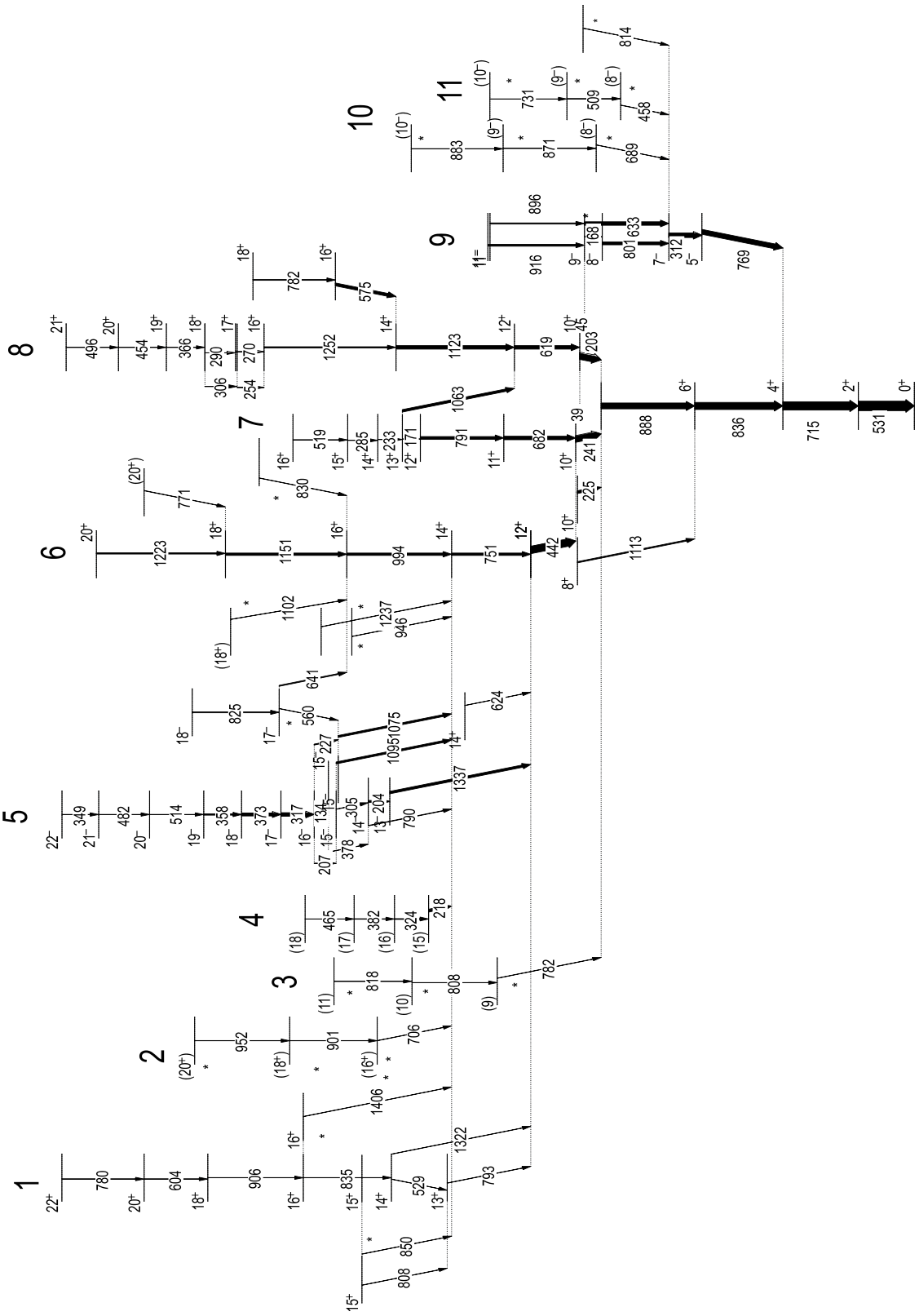

Fig. 2. Level scheme of ^{140}Sm.

Band 1 is connected to the 12^+ state of band 6, via 793 and 1322 keV γ-rays which are of dipole and quadrupole nature, respectively. Band 1 is built in the 13^+ state. The 1322 keV γ-ray was not reported in coincidence with 906 and 604 keV γ-rays by S. Lunardi et al [9]. But it is confirmed by setting double gate on 604 and 906 keV transitions that these transitions are in good coincidence with each other as shown in Fig. 3. Modification has been done in the level scheme with the placement of 529 keV (14^+ - 13^+) γ-ray in coincidence with 793 keV γ-ray. The 850 keV γ-ray connects 15^+ state to 13^+ and 808 keV γ-ray connects 15^+ to 14^+ level. The 835, 906, 604, and 780 keV γ-rays are placed in the cascade in the order of decreasing intensity as reported in Table 1.

Table 1. **Energies (E_γ), relative intensities (I_γ), RDCO values, spin assignments, and multipolarities of transitions in ^{140}Sm. Errors in E_γ are 0.3 keV for $I_\gamma > 100$, and 0.7 keV for $I_\gamma < 100$**

E_γ, keV	I_γ	RDCO	Gating transition	Multipolarity	$J_f^\pi \to J_i^\pi$
39					$10^+ \to 10^+$
44.6					$10^+ \to 9^-$
134.0	52(5)	1.37(16)			$16^- \to 15^-$
168					$9^- \to 8^-$
171.4	14(3)			M1/E2	$13^+ \to 12^+$
202.8	318(17)	1.14(9)	Q	E2	$10^+ \to 8^+$
204	96(7)				$14^- \to 13^-$
206.7					
218.2	33(3)	0.49(7)	Q		$(15 \to 14)$
225.2	35(4)	0.91(14)	Q	E2	$10^+ \to 8^+$
226.9		1.05(15)			$16^- \to 15^-$
241.2	241(15)	1.01(6)	Q	E2	$10^+ \to 8^+$
254.0	11(2)	0.41(10)	Q	M1	$17^+ \to 16^+$
269.6	14(3)	0.41(10)	Q	M1	$17^+ \to 16^+$
285.3	26(3)			M1/E2	$15^+ \to 14^+$
289.5	7(2)	0.26(6)	Q	M1/E2	$18^+ \to 17^+$
305	16(3)	0.43(10)	Q		$15^- \to 14^-$
306	12(2)				$18^+ \to 17^+$
311.6	202(14)	1.23(10)	Q	E2	$7^- \to 5^-$
317.3	90(8)	0.45(6)	Q	M1	$17^- \to 16^-$
324.3	30(4)	0.26(4)	Q		$(16 \to 15)$
348.7	3(1)			M1	$22^- \to 21^-$
358.1	30(4)	0.44(8)	Q	M1	$19^- \to 18^-$
366.4	13(3)	0.28(6)	Q	M1/E2	$19^+ \to 18^+$
373.5	49(5)	0.40(5)	Q	M1	$18^- \to 17^-$
377.5	29(4)	0.33(5)	Q		$15^- \to 14^-$
381.9	19(3)				$(17 \to 16)$
441.7	621(32)	1.14(7)	Q	E2	$12^+ \to 10^+$
454.3	7(2)	1.3(3)	D	M1/E2	$20^+ \to 19^+$
458.2	29(4)	0.68(10)	Q		$(8^- \to 7^-)$
465.7	22(3)				$(18 \to 17)$
481.6	18(3)				$21^- \to 20^-$
495.5	3(1)				$21^+ \to 20^+$
509					$(9^- \to 8^-)$
513.6	29(3)	1.03(12)	D	M1	$20^- \to 19^-$
519.4	26(3)				$16^+ \to 15^+$
529	48(5)				$14^+ \to 13^+$
530.7	1000(50)	1.10(4)	Q	E2	$2^+ \to 0^+$
559.6	14(3)				$17^- \to 15^-$
575.2	38(4)	1.13(14)	Q	E2	$16^+ \to 14^+$
603.8	60(5)	0.86(12)	Q	E2	$20^+ \to 18^+$
618.9	115(7)	1.08(8)	Q	E2	$12^+ \to 10^+$
624.2	14(3)	0.91(20)	Q	E2	$14^+ \to 12^+$
633.4	25(3)	0.75(12)	Q	M1/E2	$8^- \to 7^-$
640.9	38(5)	0.47(8)	Q	E1	$17^- \to 16^+$
681.7	44(5)	0.19(4)	Q	M1/E2	$11^+ \to 10^+$
689.3	33(3)	0.49(7)	Q		$(8^- \to 7^-)$
706	15(3)	0.83(25)	Q	E2	$(16^+ \to 14^+)$
714.9	900(45)	1.03(4)	Q	E2	$4^+ \to 2^+$
731	29(3)	0.58(7)	Q		$(10^- \to 9^-)$
751.1	377(18)	1.06(5)	Q	E2	$14^+ \to 12^+$
768.6	202(15)	0.57(5)	Q	E1	$5^- \to 4^+$

Continuation of Table 1

E_γ, keV	I_γ	RDCO	Gating transition	Multipolarity	$J_f^\pi \to J_i^\pi$
771.1	5(1)	0.99(25)	Q	E2	$(20^+ \to 18^+)$
780.3	5(1)	0.90(23)	Q	E2	$22^+ \to 20^+$
782.5	22(3)	1.12(18)	Q	E2	$18^+ \to 16^+$
782.5	10(1)				$(9 \to 8)$
790.5	12(2)	0.63(11)	D	M1/E2	$12^+ \to 11^+$
792.6	14(3)	0.18(5)	Q	M1/E2	$13^+ \to 12^+$
801.2	122(8)	0.85(4)	Q	E2	$9^- \to 7^-$
808.3	16(3)	1.02(22)	Q	E2	$15^+ \to 13^+$
808	9(2)	0.52(12)	Q		$(10 \to 9)$
814.4	9(2)	0.52(12)	Q		$\to 7^-$
817.6	14(3)	0.45(15)	Q		$(11 \to 10)$
825.3	30(3)	0.44(6)	Q	M1	$18^- \to 17^-$
830	14(3)				$\to 16^+$
835.3	69(5)	0.96(10)	Q	E2	$16^+ \to 14^+$
836.1	789(40)	1.03(4)	Q	E2	$6^+ \to 4^+$
850.4	15(3)				$15^+ \to 14^+$
870.6	29(4)				$(9^- \to 8^-)$
883.0					$(10^- \to 9^-)$
887.6	665(38)	1.10(6)	Q	E2	$8^+ \to 6^+$
895.8	26(3)	0.82(12)	Q	E2	$11^- \to 9^-$
906.1	22(4)	1.3(3)	Q	E2	$18^+ \to 16^+$
916.4	19(3)	0.89(18)	Q	E2	$11^- \to 9^-$
946.3	4(1)				$\to 14^+$
952.2	13(2)	1.24(21)	Q	E2	$(20^+ \to 18^+)$
993.6	127(8)	1.15(10)	Q	E2	$16^+ \to 14^+$
1020	9(2)				
1063.2	18(3)	0.36(6)	Q		$13^+ \to 12^+$
1074.6	45(4)	0.52(6)	Q	E1	$15^- \to 14^+$
1094.9	34(4)	0.74(12)	Q	E1	$15^- \to 14^+$
1102	3(1)				$(18^+ \to 16^+)$
1113					$8^+ \to 6^+$
1123.4	76(6)	0.96(12)	Q	E2	$14^+ \to 12^+$
1151.2	36(4)	1.10(16)	Q	E2	$18^+ \to 16^+$
1223.1	11(2)	0.90(24)	Q	E2	$20^+ \to 18^+$
1237	11(2)				$\to 14^+$
1251.5	22(3)	1.15(18)	Q	E2	$16^+ \to 14^+$
1322.3	22(3)	1.30(20)	Q	E2	$14^+ \to 12^+$
1336.9	57(5)	0.59(7)	Q	E1	$13^- \to 12^+$
1406.1	7(1)	0.9(2)	Q	E2	$16^+ \to 14^+$

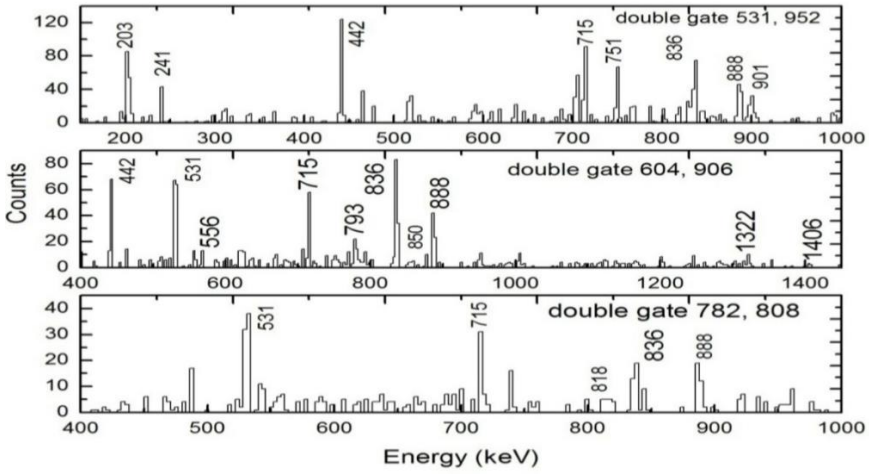

Fig. 3. Double-gated coincidence spectra for ^{140}Sm.

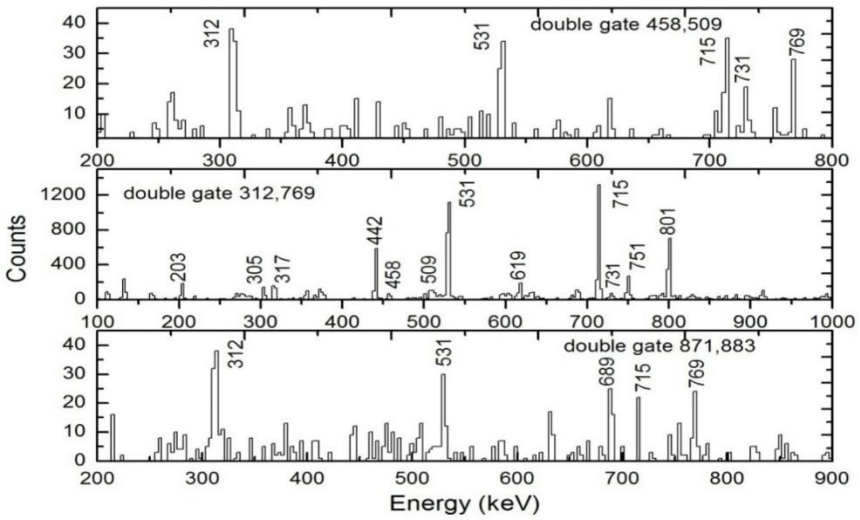

Fig. 4. Double-gated coincidence spectra in ^{140}Sm.

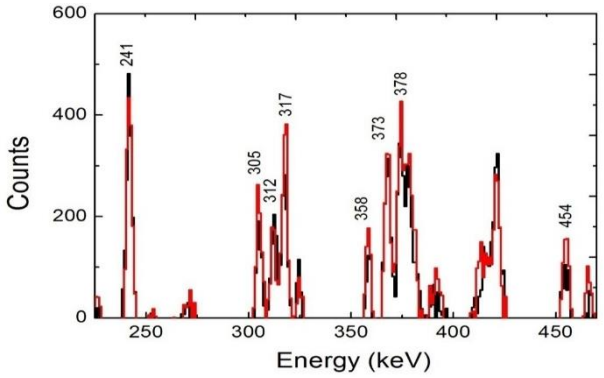

Fig. 5. Comparison of parallel and perpendicular scattered events in ^{140}Sm. (See color Figure on the journal website.)

Bands 2 and 3, which are weakly populated, are established from the present work. Band 2 consists of a regular cascade of 706, 901, and 952 keV transitions. From DCO ratio measurements, these transitions are of quadrupole nature. The transition connecting to 14^+ is also quadruple type. Band 3 consists of cascades of 782, 808, and 818 keV γ-rays and are of dipole nature, concluded from DCO measurements. Parities of these states are not confirmed because they are weakly populated and IPDCO measurements are not possible. Band 4 was tentatively placed in the previous work [9]. Spins of this band have been assigned in the present work by RDCO measurements. The 218 keV γ-ray connecting band 4 to the 12^+ state of band 6 is of dipole nature.

Band 5 is of a dipole nature with negative parity. Spins and parities of 317, 373, 358, 514, and 482 keV transitions have been assigned using DCO and IPDCO measurements and are magnetic in nature. The 1337 keV transition connects 13^- state to 12^+ state of band 6 and is E1 in nature. The 1075 and 1095 keV transitions connect 15^- state to 14^+ state. The intense band 6 above the 10^+ state at 3200 keV with $T_{1/2}$ = 6.2 ns was assigned $(\pi h_{11/2})^2$ configuration from the systematics of the 10^+ states in the N = 78 isotones and from the comparison with the ^{136}Ce configuration. We confirm nearly all transitions observed in Ref. [9]. The 771, 830, 946, 1102, and 1237 keV γ-rays are observed in the present study connecting to the states of this quadrupole band. A particular feature of the level scheme of ^{140}Sm at medium spins is the existence of cascades of dipole transitions. Band 7 is a dipole band. Transitions connecting the states of this band are of mixed nature (M1/E2).

Band 8 at 3172 keV above the 10^+ state has been assigned $(\nu h_{11/2})^{-2}$ with $T_{1/2}$ = 22.3 ns. There is a cascade of E2 transitions from 10^+ to 16^+. Above 16^+, transitions connecting to high spin states are observed in the present work. Transitions of 270, 290, 306, 366, and 454 keV are of mixed nature (M1/E2). In the present study, spins and parities of high spin states above 16^+ have been assigned. Sequence 9, which decays by an E1 γ-ray (769 keV) to the last band is developed on the 5^- level (2015 keV) and extends up to 11^- (4044 keV). Bands 10 and 11, which are weakly populated, have been established from the present study.

6. Configuration of various bands

Experimental alignments, $i_x = I_x - I_{xref}$ for different bands are plotted in Fig. 6 as a function of rotational frequency. Here I_x was estimated as $I_x = [(I + 1/2)^2 - K^2]^{1/2}$. I_{xref} is based on the frequency-dependent variable moment of inertia reference, $\Im_{ref} = \Im_0 + \Im_1 \omega^2$ where Harris parameters $\Im_0 = 8.9\ \hbar^2\ \text{MeV}^{-1}$ and $\Im_1 = 14.8\ \hbar^4\ \text{MeV}^{-3}$ are used [16]. A band structure similar to ^{140}Sm has been found in ^{136}Ce. So, the alignment in both the nuclei is compared for various band structures having similar band head spin.

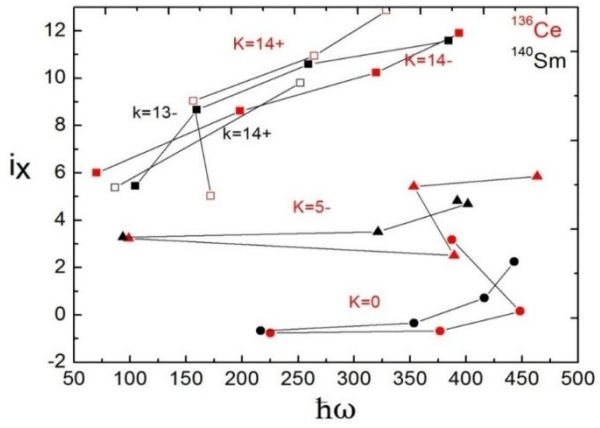

Fig. 6. Experimental alignment for ^{140}Sm and ^{136}Ce. (See color Figure on the journal website.)

As already pointed out in the introduction, the excited states in ^{140}Sm nucleus above the proton and neutron $h^2_{11/2}$ isomers have been successfully interpreted up to 16^+ as the core states coupled to the 10^+ single-particle excitations. Band 5 based on 14^- has been assigned 4-quasiparticle configuration $\pi[g_{7/2}, h_{11/2}] \otimes \nu[h_{11/2}]^{-2}$. The results of TAC [17] calculations for band 5 are shown in Fig. 7. This configuration resulted in the minimum total energy at deformation $\varepsilon_2 \approx 0.108$ and $\gamma \approx 51°$ with TAC angle $\approx 30°$. The pairing for proton, $\delta_p = 1.191$ MeV and neutron, $\delta_n = 0.958$ MeV was calculated from the atomic mass table 2012 [18]. The experimental behaviour of I versus ω matches with TAC model calculations. B(M1) and B(M1)/B(E2) behaviour predicted by the TAC model is shown in Fig. 7.

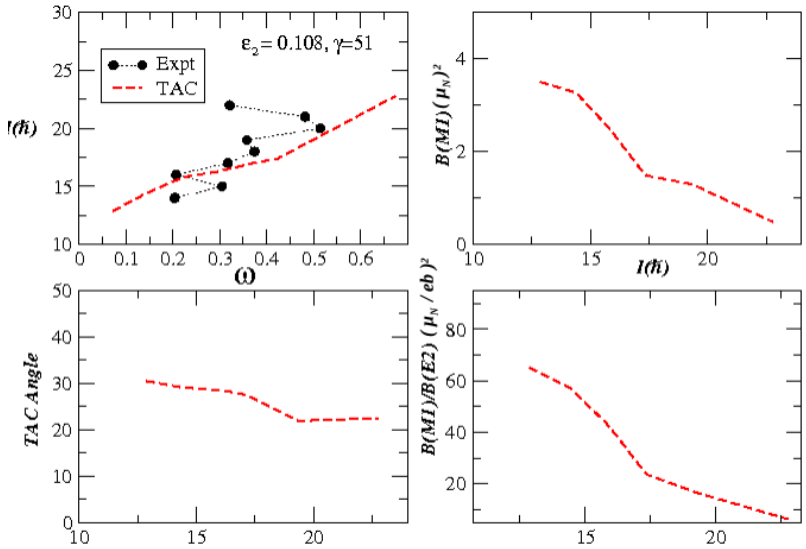

Fig. 7. The *upper panel* – the dependence of the angular momentum I(ħ) on the rotational frequency ω and B(M1) values versus spin I(ħ). The *lower panel* – the TAC angle and B(M1)/B(E2) ratio versus I(ħ). (See color Figure on the journal website.)

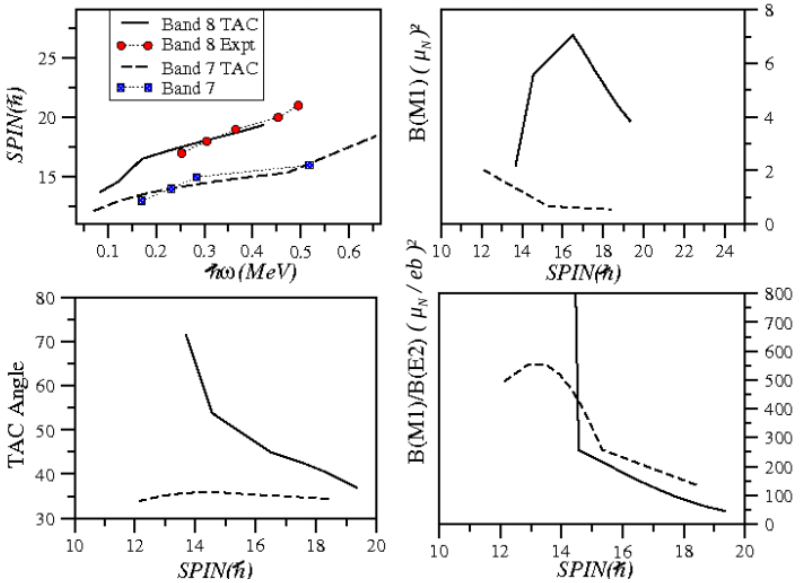

Fig. 8. The *upper panel* – the dependence of the angular momentum I(ħ) on the rotational frequency ω and B(M1) values versus spin I(ħ). The *lower panel* – the TAC angle and B(M1)/B(E2) ratio versus I(ħ) for bands 7 and 8. (See color Figure on the journal website.)

Lifetime information of the states is necessary to confirm experimental B(M1) values. TAC calculations for bands 7 and 8, with pairing for proton 1.191 MeV and for neutron 0.958 MeV (80 % of pairing from masses with 2012 mass table), have been performed. For band 7 the configuration assigned from systematic seems to be $\pi[g_{7/2}, h_{11/2}] \otimes \nu[g_{7/2}, h_{11/2}]$ and resulted in total energy minimum at deformation, $\varepsilon_2 = 0.100$ and $\gamma = 30°$, here TAC angle is very stable with average value about 35°.

The I versus ω behaviour for this configuration is displayed in Fig. 8 with the dashed line. For band 8, the configuration is $\pi[h_{11/2}]^2 \otimes \nu[h_{11/2}]^{-2}$ with minimum at $\varepsilon_2 = 0.140$, $\varepsilon_4 = 0.012$ and $\gamma = 58°$. At low frequency, the band nearly obeys principal axis cranking which is seen experimentally with the observation of strong E2 transition below 14^+. Also, it has low values of B(M1)/B(E2) at high spins (above 17^+) which suggests that we should observe the E2 transition for this band at high spins. However, we are not able to place such E2 transitions in the present study. The low-lying negative parity states of band 9 were assigned two neutron configurations, $\nu[h_{11/2}, s_{1/2}/d_{3/2}]$ from the energy information of 5^- states in Ba [19] and Nd isotopes [1].

7. DSAM lifetime measurements

Lifetimes of states have been measured by the Doppler shift attenuation method. For this, asymmetric matrices were constructed by keeping the 65° detector on one axis and the rest of the detectors on the other axis for forward analysis. For backward line-shape analysis, −65°(115°) detectors were kept on one axis and the rest of the detectors on another axis. Similar matrices were constructed for detectors placed at +40° and −40°. To check the contamination in forward and backward data, matrices were constructed for 90° versus all detectors. For line-shape analysis of the transitions, the LINESHAPE program [20] was used. The program takes into account the energy loss of the beam through the target, the energy loss, and the angular straggling of the recoils through the target and the backing. For the energy loss, we used the shell-corrected Northcliffe and Schilling stopping powers [21]. The value of the time step and the number of recoil histories were chosen to be 0.001 ps and 5000, respectively. Apart from the mass and density profile of the projectile and target, the inputs of code DECHIST and HISTAVER are: target to detector distance, which is 25 cm in our case, and the radius of the Ge-detector, which is 6 cm. Fitting was started at the top level with all the parameters of other levels kept fixed. Once the χ^2 minimization was achieved by the MINUIT program, the background and the contaminant peak parameters were fixed, and the procedure was followed for the next lower level.

After obtaining χ^2 minimization for each level, a global fit was carried out, with the background and the contaminant peak parameters of all the levels kept fixed. However, it should be noted that quoted errors do not include systematic errors in stopping power values which may be as large as 20 %. Fig. 9 displays χ^2 fit for 1151 and 994 keV γ-rays.

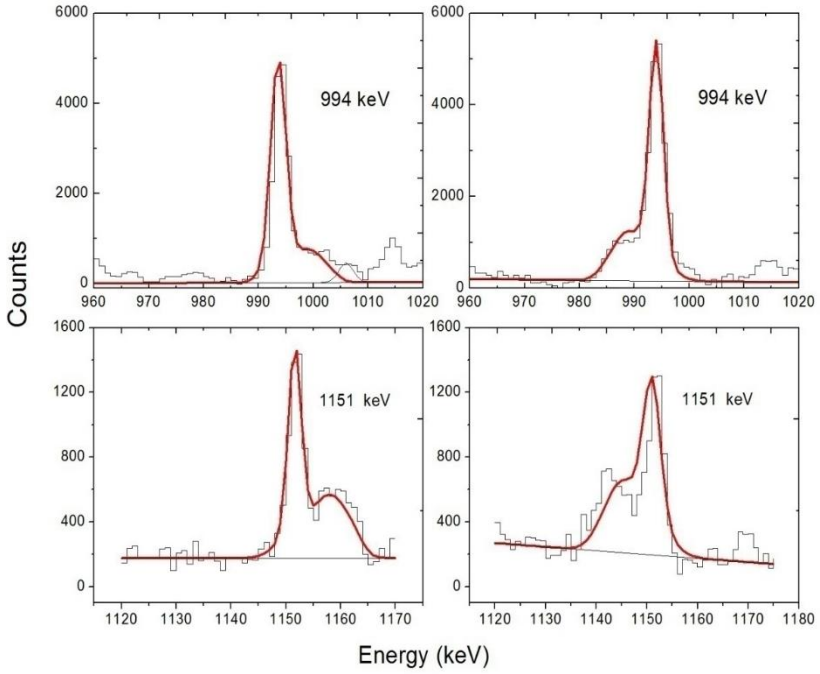

Fig. 9. Results of χ^2 fits of the line shape analysis.

Table 2. **Lifetime and B(E2) values of quadrupole bands in ^{140}Sm. Error bars on measured lifetimes include fitting errors and errors inside feeding intensities**

E_γ, keV	I^π	T, ps	B(E2) (e^2b^2)
994	16^+	$2.47^{+0.1}_{-0.1}$	$0.034^{+0.001}_{-0.001}$
1151	18^+	$1.32^{+0.07}_{-0.07}$	$0.031^{+0.002}_{-0.002}$
442	12^+	22	
619	12^+	11	
751	14^+	1.7	

The B(E2) values are calculated using the following equation

$$B(E2)=\frac{0.0816B_\gamma(E2)}{E_\gamma^5(E2)\tau\left[1+\alpha_t(E2)\right]}(eb)^2. \quad (2)$$

Earlier lifetime measurements in ^{140}Sm have been carried out by M.A. Cardona et al. [13] using the RDM technique for 12^+ and 14^+ states and are listed in Table 2. The values quoted for lifetime in Table 2 for 442 keV ($12^+\rightarrow10^+$), 619 keV ($12^+\rightarrow10^+$), and 751 keV ($14^+\rightarrow12^+$) are taken from reference [13].

5. Summary

In the present work, high-spin states in ^{140}Sm have been investigated using the INGA facility at TIFR, Mumbai following the ^{116}Cd (^{28}Si, 4n) ^{140}Sm heavy ion fusion evaporation reaction. The level scheme has been modified with the addition of several new transitions. The DCO and IPDCO were calculated to assign the spins and parities to the levels. The lifetimes of various levels have been determined using the LINESHAPE program. The TAC model calculations have been performed for bands 5, 7, and 8. The band 5 has been assigned 4-quasiparticle configuration, i.e., $\pi[g_{7/2}, h_{11/2}] \otimes \nu[h_{11/2}]^{-2}$. For bands 7 and 8, the configurations were assigned from systematic and found to be $\pi[g_{7/2}, h_{11/2}] \otimes \nu[g_{7/2}, h_{11/2}]$ and $\pi[h_{11/2}]^2 \otimes \nu[h_{11/2}]^{-2}$, respectively.

REFERENCES

1. C.M. Petrache et al. Evolution from spherical single-particle structure to stable triaxiality at high spins in ^{140}Nd. Phys. Rev. C 72 (2005) 064318.
2. N. Redon et al. New exotic neutron-deficient nuclei near N = 82. Z. Phys. A 325 (1986) 127.
3. A.A. Pasternak et al. Investigation of lifetimes in the dipole band of ^{139}Sm. Eur. Phys. J. A 37 (2008) 279.
4. F. Brandolini et al. Lifetimes of a shears band in ^{139}Sm. Phys. Lett. B 388 (1996) 468.
5. S. Muralithar et al. Indian National Gamma Array at Inter University Accelerator Centre, New Delhi. Nucl. Instrum. Methods A 622 (2010) 281.
6. V.S. Barashenkov, B.F. Kostenko, A.M. Zadorogny. Time-dependent intranuclear cascade model. Nucl. Phys. A 338 (1980) 413.
7. R. Palit et al. A high speed digital data acquisition system for the Indian National Gamma Array at Tata Institute of Fundamental Research. Nucl. Instrum. Methods A 680 (2012) 90.
8. D.C. Radford. ESCL8R and LEVIT8R: Software for interactive graphical analysis of HPGe coincidence data sets. Nucl. Instrum. Methods. A 361 (1995) 297.
9. S. Lunardi et al. Excited states in ^{140}Sm above the $(\pi h_{11/2})^2$ and $(\nu h_{11/2})^{-2}$ 10^+ isomers. Phys. Rev. C 42 (1990) 174.
10. E.O. Lieder et al. Investigation of lifetimes in quadrupole bands of ^{142}Gd. Eur. Phys. J. A 35 (2008) 135.
11. C.M. Petrache et al. Tilted axis rotation, candidates for chiral bands, and wobbling motion in ^{138}Nd. Phys. Rev. C 86 (2012) 044321.
12. S. Lakshmi et al. High spin structure of ^{136}Ce. Nucl. Phys. A 761 (2005) 1.
13. M.A. Cardona et al. Shape coexistence in ^{140}Sm and the onset of deformation below N = 82 from lifetime measurements. Phys. Rev. C 44 (1991) 891.
14. A. Krämer-Flecken et al. Use of DCO ratios for spin determination in γ-γ coincidence measurements. Nucl. Instrum. Methods. A 275 (1989) 333.
15. N. Kaur et al. High spin structure in ^{130,131}Ba. Eur. Phys. J. A 50 (2014) 5.
16. E.S. Paul et al. Shape coexistence in ^{138}Sm and evidence for the rotational alignment of a pair of N = 6 neutrons. J. Phys. G 20 (1994) 1405.
17. J.A. Sheikh. Tilted-axis cranking analysis in a simple model. Phys. Rev. C 52 (1995) 3061.
18. M. Wang et al. The AME2012 atomic mass evaluation (II). Tables, graphs and references. Chinese Phys. C 36 (2012) 1603.
19. O. Vogel et al. High spin states in ^{128}Ba. Eur. Phys. J. A 4 (1999) 323.
20. J.C. Wells, N.R. Johnson, LINESHAPE: A computer program for Doppler-broadened lineshape lifetime analysis. Oak Ridge National Laboratory Physics Division Progress Report No. ORNL-6689, September 30 (1991) p. 44.
21. L.C. Northcliffe, R.F. Schilling. Range and stopping-power tables for heavy ions. Nucl. Data Tables 7 (1970) 233.

Б. Рохіла[1], Н. Каур[2,*]

[1] *Фізичний факультет, Коледж Майтрея, Делійський університет, Делі, Індія*
[2] *С. А. Джайн Коледж, місто Амбала, штат Хар'яна, Індія*

*Відповідальний автор: nvneet86@gmail.com

ВИСОКОСПІНОВА СТРУКТУРА В ^{140}Sm

Високоспінові стани ^{140}Sm були заселені за допомогою реакції злиття важких іонів з випаровуванням ^{116}Cd (^{28}Si, 4n) ^{140}Sm. Відома раніше схема рівнів була значно модифікована та розширена. Призначення спіну та парності було зроблено за допомогою методів DCO та IPDCO. Багатоквазічастинкові конфігурації були призначені різним $\Delta I = 1$ і $\Delta I = 2$ смугам на основі систематики. Структура смуг, подібна до ^{140}Sm, була знайдена в ^{136}Ce. Таким чином, структура в обох ядрах порівнюється для різних смуг, що мають подібний головний спін. Це допомагає визначити конфігурацію різних смуг. Структури рівнів обговорювалися в рамках моделі TAC. Тривалість життя станів була виміряна за допомогою методу DSAM.

Ключові слова: γ-γ збіг, Індійська національна гамма-решітка (INGA), спектроскопія, RDCO, DSAM.

Надійшла / Received 24.04.2024